Journal Pre-proof

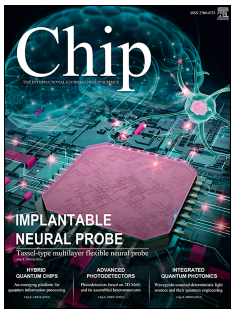

Sensing with extended gate negative capacitance ferroelectric field-effect transistors

Honglei Xue, Yue Peng, Qiushi Jing, Jiuren Zhou, Genquan Han, Wangyang Fu

PII: S2709-4723(23)00037-0

DOI: https://doi.org/10.1016/j.chip.2023.100074

Reference: CHIP 100074

To appear in: *Chip*

Received Date: 23 August 2023

Revised Date: 22 October 2023

Accepted Date: 13 November 2023

Please cite this article as: Xue H, Peng Y, Jing Q, Zhou J, Han G, Fu W, Sensing with extended gate negative capacitance ferroelectric field-effect transistors, *Chip*, https://doi.org/10.1016/j.chip.2023.100074.

Sensing with extended gate negative capacitance ferroelectric field-effect transistors

Honglei Xue[1]#, Yue Peng[2]#, Qiushi Jing[1], Jiuren Zhou[2], Genquan Han[2]*, Wangyang Fu[1]*

[1]Key Laboratory of Advanced Materials (MOE), School of Materials Science and Engineering, Tsinghua University, Beijing 100084, People's Republic of China

[2]School of Microelectronics, Xidian Univeristy, Xi'an 710071, People's Republic of China

*E-mail address: gqhan@xidian.edu.cn; fwy2018@mail.tsinghua.edu.cn

ABSTRACT

With major signal analysis elements situated away from the measuring environment, extended gate (EG) ion-sensitive field effect transistors (ISFETs) offer prospects for whole chip circuit design and system integration of chemical sensors. This work presents the formulation of a highly sensitive and power-efficient ISFET based on a metal-ferroelectric-insulator gate stack with negative capacitance (NC)-induced super-steep subthreshold swing and ferroelectric memory function. Along with a remotely connected extended gate electrode, the architecture facilitates diverse sensing functions for future establishment of smart biochemical sensor platforms.

Keywords: Extended gate, Ion-sensitive field-effect transistors, Negative capacitance, Sub-60 mV/dec subthreshold swing, Ferroelectric memory effect

INTRODUCTION

The integration of sensing, memory and computing (IoSMC), is of vital importance to meet the challenges in Internet-of-Things (IoT) and Artificial Intelligent (AI)[1-3]. Extended gate (EG) ion-sensitive field-effect transistors (ISFETs) lay a solid foundation for pursuing the development of such highly desired smart biochemical sensor platforms[4]. That is, by isolating the transistors from the test environment, EG ISFETs offer whole chip circuit design and system integration for improved sensitivity, long-term stability and reliability[5, 6]. Specific detection can be customized by functionalization of the EG. Thanks to the separation of the sensing environment from the chips, EG ISFETs not only can help mitigate drift, degradation and aging, suppress noise and ensure stable and reliable sensing response, but also facilitate sensor cleaning and recycling, thus reducing costs and minimizing environment impact[7].

Negative capacitance ferroelectric field-effect transistors (NC FeFETs), are promised to overcome the limitations of

traditional metal-oxide-semiconductor FET (MOSFET), specifically the Boltzmann-defined lowest subthreshold swing, i.e. 60 mV/decade at room temperature[8-11]. In addition, external electric field triggered polarization switching in ferroelectric materials can contribute to distinct non-volatile states ("ON" and "OFF" states)[12-14], thus opening up new possibilities on IoSMC by utilizing the gating effect of the ferroelectric polarization field on the charge transport of the semiconducting channel.

Nevertheless, traditional ferroelectric materials suffer from the critical dimension problem, which limits their valuable ferroelectricity at the nanometer scale and represents an obstacle for improving the transistor performance as well as the computing and sensing capabilities[14-17]. Therefore, NC FeFETs based on two-dimensional (2D) ferroelectric ultrathin films scaled down to several nanometers is highly promising[18]. Particularly, hafnium zirconium oxide ($HfZrO_x$, HZO) achieved via complementary MOS (CMOS) compatible atomic layer deposition (ALD) technology[19-21], possesses relatively high-κ and large bandgap and is an innovative candidate for the development of modern FeFETs[22-26] and advanced sensors [27-29].

In this work, we propose a highly sensitive and power-efficient ISFET based on a metal-ferroelectric-insulator (MFI) gate stack. Here, we employed a 6 nm HZO as the ferroelectric layer, along with a 2-nm-thick AlO_x buffer layer, to construct an MFI gate stack on p-type silicon or highly n doped germanium. This design allows to harvest the NC effect and the ferroelectric memory effect with reduced operation voltage for sensing applications[30]. We successfully characterized the NC effect, achieving valuable sub-60 mV/decade SS (the lowest point SS = 40 mV/dec) and the desired ferroelectric loop, in the fabricated MFI-semiconductor (MFIS) FeFETs. Further ionic sensing measurements are applied on this NC FeFET with EG. Schematic illustration of the sensing platform and the polarization states originated from different gating effect are shown in Fig.1a and 1b, respectively. In principle, the ferroelectric polarization state in the HZO layer changes according to the polarity of the applied gate voltage. Furthermore, different sensing environment with charged molecules around the reference electrode can modulate the applied voltage on the HZO according to the charge detection principle of ISFETs. Therefore, the ferroelectric polarization will be modulated by the environment. Fig. 1c illustrates a typical transfer curve of NC FeFET with a clockwise ferroelectric memory window. The device's 'OFF' state exhibits dominant downward polarization. In the presence of charged molecules including pH, ions, DNAs and proteins, the 'OFF' state device can be switched 'ON' under the same gate voltage as represented by the dashed red line interception, due to a potential positive shift of the V_{th}. Such upward polarization state is nonvolatile and can be maintained unless it is intentionally erased or programed by applying an external gate voltage that surpasses the positive coercive reset voltage. Therefore, the presence of charged molecules can be detected and recorded even if the sensing environment comes back to its original conditions, signifying the potential of FeFETs for smart sensing. At the end of our study, we find that when the potassium ion concentrations changes from 1 mM to 1 M, it reveals high sensitivity of

62 (±2) mV/decade, which is superior to that of 48 mV/dec of its MOSFET counterparts[31, 32]. Along with configurable ferroelectric memory windows, we envision potential development of NC FeFETs towards future IoSMC applications.

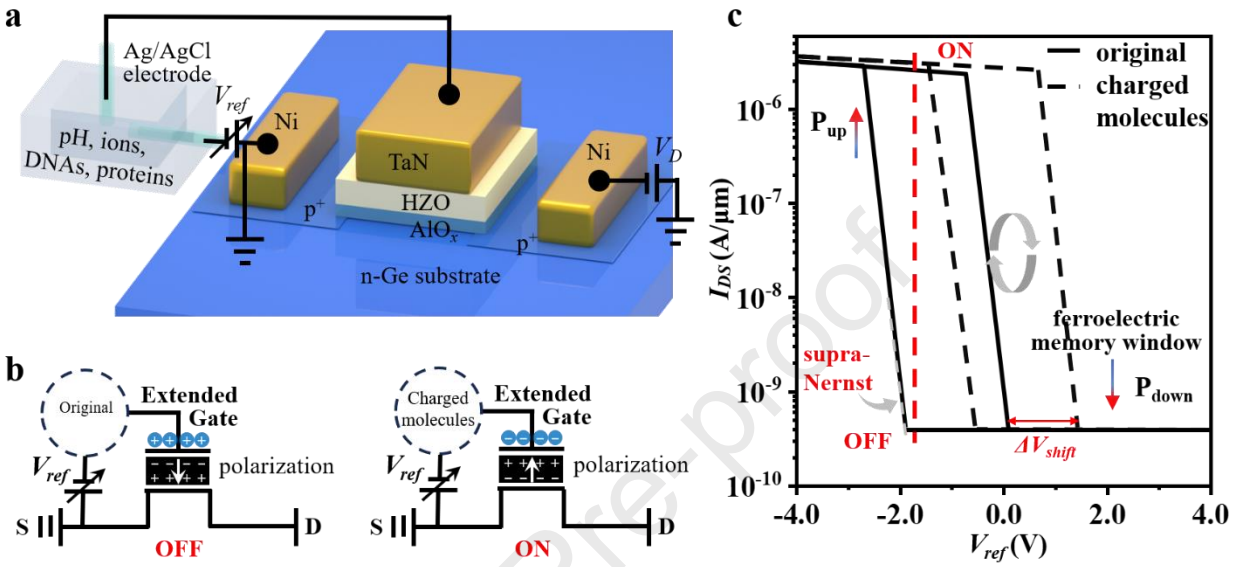

Fig. 1 | Sensing platform and schematic of smart sensing modulation. a, Illustration of the smart sensing measurement on EG NC FeFETs. **b,** Schematic diagrams of the ferroelectric gating effect on EG NC FeFETs. Charges with opposite sign to the gate are accumulated on the interface between the gating electrode and the ferroelectric layer. Different gating states lead to different polarization states. **c,** Schematic image of the ideal smart sensing state originated from different sensing environment. The black solid line indicates the original device state and the black dashed line gives the transfer curve of devices in pH/ions, in which original device gives an "OFF" state and in the presence of charged molecules, the device presents an "ON" state at the same gating condition (the red line).

MATERIALS AND METHODS

In Fig. 2a, we present the optical image and the cross-section schematic structure of the MFISFET arrays. A sub-10 nm gate dielectric stack constituted of 2 nm AlO_x and 6 nm HZO was adopted on either p-type Si or n-type Ge substrates using an atomic layer deposition (ALD) tool. Prior to deposition, pure n-type Ge (or p-Si) surface was firstly cleaned with acetone, methanol and deionized water in an ultrasonic bath for 15min respectively, passivated with 10 cycles Al_2O_3 and then treated with O_3 atmosphere for 20 minutes to form a 2 nm AlO_x layer. Here, AlO_x was built up as a gate buffer layer to provide performance enhancement. Two major restrictions in FeFETs including gate leakage current and charge traps can be better improved through the AlO_x buffer layer[12, 33-35]. Extra 6 nm high-quality HZO layer with a Zr/Hf ratio of 1:1 was grown on the AlO_x layer by ALD. A TaN layer (100 nm) was deposited by sputtering as the gate electrode. Boron ions (B^+) for and

phosphorous ions (P^-) were implanted into the source/drain electrode areas for Ge and Si channel transistors, respectively. The implantation energy was 20 KeV and the dose was 10^{15} cm^2. Ni (20-30 nm) was deposited into the source/drain(S/D) regions to form the metallic S/D contacts. Finally, the devices were accomplished by a 30 seconds post annealing at 450 ℃. Indeed, in our prior studies, we have examined orthorhombic phase in HZO[36]. XRD curves that we have obtained suggests mixed phases within HZO after undergoing annealing at 450 ℃ for 30 s. This includes the presence of a partial orthorhombic phase. To confirm the MFIS gate dielectric core structure, cross-sectional transmission electron microscopy (TEM) was made on a representative device (Fig.2b, comparable MFS structure in Fig. S1). According to the TEM profile image, all interfaces between every two layers are flat and clear, validating the integrity of the MFIS gate dielectric core structure. While it is admittedly challenging to identify the orthorhombic phase[37] in FFT of the TEM image showcased in Fig. 2b. We are of the opinion that the analysis via XRD, in conjunction with the electrical P-E measurements, is adequate to ascertain the ferroelectric properties of HZO.

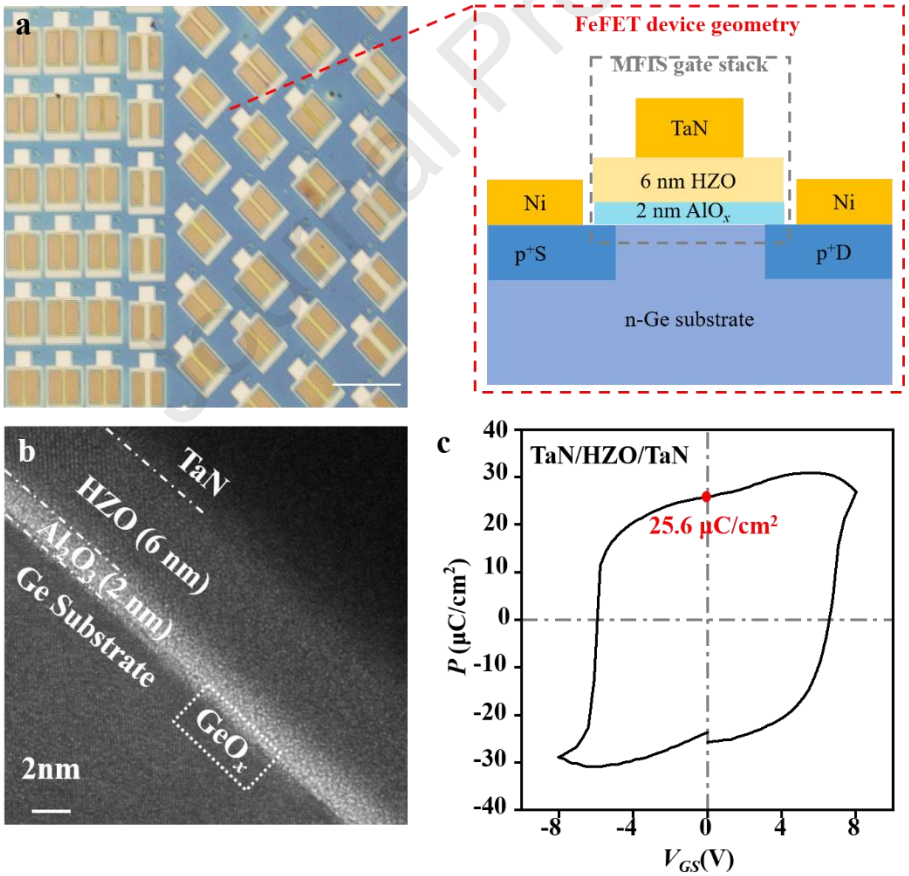

Fig. 2 | The 6 nm HZO ferroelectric gate dielectric layer MFISFET device structure and ferroelectricity characterization. a, Optical image of 6 nm HZO ferroelectric FET arrays and schematic diagram of the HZO ferroelectric FET gate stack cross-section. Scale bar, 200 μm. **b,** Transmission electron microscopy (TEM) image

showing the profile of TaN/HZO/Al_2O_3 gate stack of a representative device. Scale bar, 2 nm. **c,** Ferroelectric hysteresis loop of 6 nm HZO ferroelectric film (TaN/HZO/TaN).

RESULTS AND DISCUSSIONS

Ferroelectric properties embodied in, for example, the ferroelectric *P-V* hysteresis loop and the NC effect, are of key importance in the electrical characterizations of NC FeFETs. In our study, we observed a robust ferroelectric polarization response is from metal-ferroelectric HZO film-metal (MFM) *P-V* measurement. Fig. 2c depicts the *P-V* hysteresis loop with a remnant polarization (P_r) of 25.6 μC/cm^2. Fig. S2 demonstrates an additional ferroelectric hysteresis loop of 10 nm HZO with switching current.

Fig. 3a presents the output curves of a typical NC FeFET device with a 5 μm gate length (L_G). Notably, the device exhibits a negative differential resistance (NDR) effect in the whole subthreshold V_{DS} region ranging from -0.4 V to -2 V (Fig. S3). One step further, we measured the transfer characteristics and depicted the corresponding SS, as shown in Fig. 3b. Strikingly, augmented by virtue of the NC effect from HZO ferroelectricity, the commendable FeFET achieves sub-60 mV/decade below the thermionic limit. That is, Fig. 3b demonstrates 3 data points below the Boltzmann limit in the subthreshold region with the lowest value of SS $= \frac{dV_G}{dlgI_{DS}}$ = 40 mV/dec, where the potential sensing response will suppress that of conventional MOSFET devices. The suppressed gate leakage current due to MFIS structure was present in Fig. S4. We note here that the fluctuations in SS (Fig. 3b) may be attributed to the switching of the multi-domains in the ferroelectric HZO thin film, as reported in our previous publications[36, 38, 39]. Such fluctuations are reproducible to a large extend, as illustrated in Fig. S5a. Similar significant SS fluctuations and none smooth transfer curves were also observed in NC FinFETs[40]. To promote further development of highly sensitive biochemical sensors with low SS value and memory functions, in the follow we exam the synergetic performance of the ferroelectric memory effect and charge trapping effect in the subthreshold region of NC FeFET devices.

Fig. 3c depicts the dual sweepings of gate voltage (V_{GS}) with various ranges (±2 V to ±4 V), lead to either counter-clockwise ferroelectric loop or clockwise hysteresis in an n-NC FeFET. Calculated SS values are shown in Fig. S6. Biased at a sufficiently large V_{GS} sweeping range of ±4 V, initial/remnant polarization can be flipped/switched and the device exhibits a significant counter-clockwise ferroelectric loop (with a memory window of 1.3 V). We also observed clockwise hysteresis due to charge trap states if biased at a small V_{GS} sweeping range of ±2 V. Whereas at a moderate V_{GS} sweeping range (±3 V), we observed a counter-clockwise loop with a relatively small ferroelectric memory window. Such changes in the direction as well as the width of the memory windows, can be ascribed to an underlying synergetic effect by taking into account both the ferroelectric polarization effect and the interfacial charge-trapping effect[41].

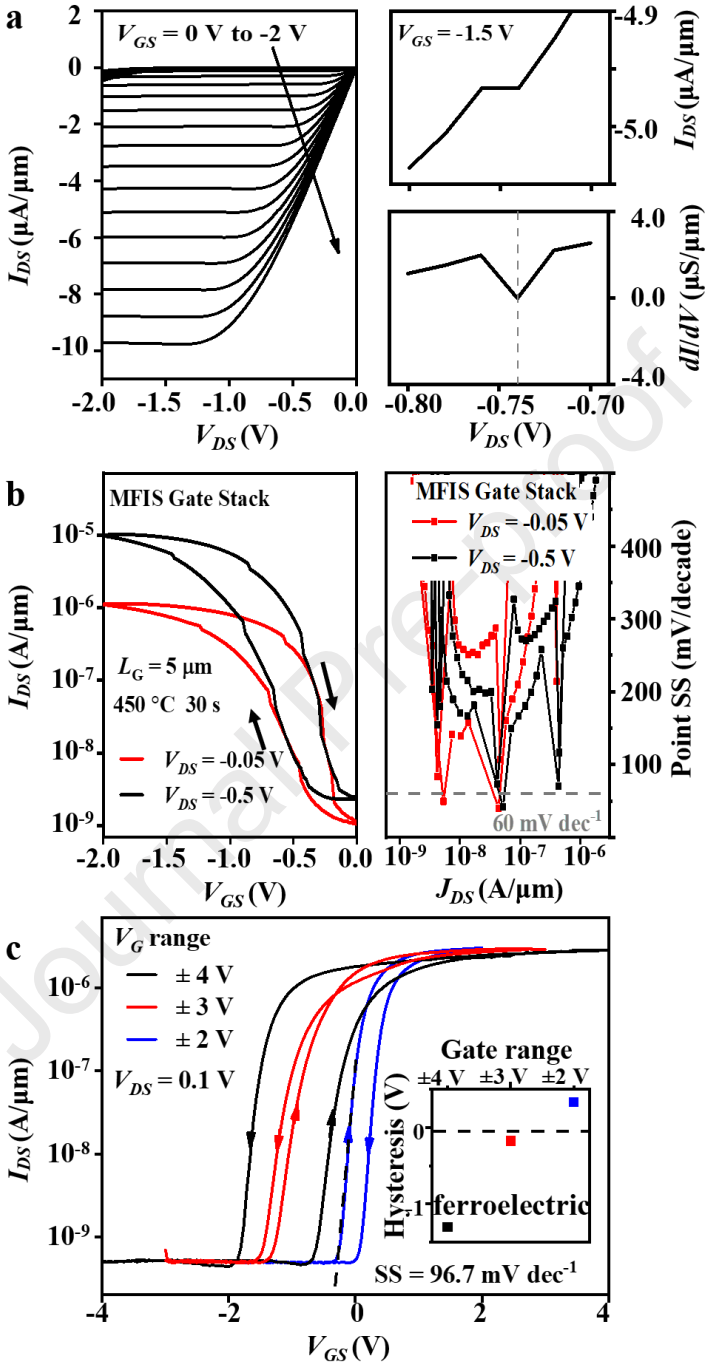

Fig. 3 | Electrical characterization of NC FeFETs. a, Left: Output characteristic curves of the p-type HZO FeFET. V_{GS} is biased form 0 V to -2 V with a step of -0.1 V. Right up: Output characteristic curve with gate bias at -1.5 V. Right down: The *dI/dV* spectra extracted from the upper curve, showing negative differential resistance. **b,** Left: Forward and reverse transfer characteristic curves under V_{DS} = -0.05 V and V_{DS} = -0.5 V, respectively. Inserted arrows show the hysteresis direction of the devices. Right: Calculated point SS according to the transfer curve. **c,** Comparison of I_{DS} as a function of top-gate voltage with different gate voltage range cycling from (±4 V, ±2 V) in steps of 1 V.

To evaluate the sensing performance of the NC FeFETs, we performed further chemical sensing experiments in aqueous solutions with various K^+ concentrations as testbeds. Fig. S7a depicts the transfer characteristics of the FeFET and the calculated SS spectra, respectively. It is important to note that the HZO ferroelectric thin film were polarized in P_{down} state, as the gate voltage (from -0.8 V to 0.8 V) were swept within the negative coercive voltage (<-2 V, Fig. 4b, see also the inset of Fig. 3c) of the HZO ferroelectric thin film. Thanks to the ferroelectricity of the nanoscale ferroelectric HZO thin film, comparably lower SS (Fig. S7b), as well as amplified voltage gating efficiency due to NC effect can be achieved advantageously[42] for ion sensing with enhanced responsivity and sensitivity. Noted that we operated the FeFET under the same gate step of 20 mV and constant output source/drain voltage V_{DS} (V_{DS} = 0.1V for n-type FETs and V_{DS} = -0.1V for p-type FETs), to exclude a possible impact of gate voltage step and source/drain applied voltage on the electrical behaviors[43-45]. Ag/AgCl reference electrode was adopted as the extended liquid gate to define the electrostatic potential in a homemade liquid chamber and then connected with the on-chip gate electrode of NC FeFETs as illustrated in Fig. 1a and S8a. Fig. 4a depicts the drain current (I_{DS}) plotted against the reference voltage (V_{ref}) in KCl solutions with increased concentrations from 1 mM to 1 M. The NC FeFET sensor yielded a stable and evident response towards positive V_{th}. We plotted the deduced threshold voltage shifts against the KCl concentrations in the inset of Fig. 4a, which exhibited a positive threshold voltage shift of 62 (±2) mV/dec, corresponding to an overall 76 times change in current at V_{ref} = -0.5 V when concentration varies from 1 mM to 1 M. The relative sensing response can be deduced as $S_{ConI} = \frac{(I_{ConI} - I_{Con,ref})}{I_{Con,ref}}$. Repeating the measurements gave stable and reproducible results. In addition, Fig. S8b illustrates that the calculated SS values here are consistent with those obtained in ambient air conditions. Our observed potassium sensitivity of 62 mV/dec even slightly exceeds the theoretical value according to the thermodynamic Nernst limit (60 mV/dec at room temperature). We ascribed the superior sensitivity beyond the Nernst limit to a capacitive effect, which can be referred to the gate voltage amplification due to ferroelectric NC effect[42]. Remarkably, unless the baseline MOSFET has ideal SS at 60 mV/decade limit, it is almost impossible to obtain sub-60 mV/decade SS. Nevertheless, better SS can be obtained in NC FET over control device no matter whether the SS is steep or not, i.e., the NC effect might not always lead to the sub-kT/q SS, but must contribute to the improved performance (SS) compared to the baseline device[46, 47]. When compare its performance with its counterparts without ferroelectric NC effect (see Fig. S7b), we can clearly identify an improvement in the SS values, suggesting the effectiveness of the NC effect from HZO.

Furthermore, smart sensing is expected based on the ferroelectric memory effect of the FeFETs. The polarization state of ferroelectric layer could be modulated by the voltage on the extended gate, as illustrated in Fig.1b. In principle, downward and upward polarization states of P_{down} and P_{up} occur under respective gate biases separated by the ferroelectric window, resulting

in a low resistance state (LRS) and a high resistance state (HRS), corresponding to logic bits "1" and "0" as indicated by the arrows in Fig. 4b, respectively. Fig. 4b gives the transfer curves of an n-NC FeFET with a relatively large counter-clockwise ferroelectric window (1.3 V), tested in ambient air as the background (black line) and against 1 mM K^+ solution (blue line) as the analyte. Here, we conceived that chemical sensing information could be stored by employing ion-modulated polarization states. The appreciable threshold voltage shift upon introducing 1 mM K^+ (270 mV) in Fig. 4b, suggests the possibility of switching the FeFET sensor from its HRS (P_{up} state) to LRS (P_{down} state) if assuming an initially bias EG voltage of -0.7 V (see the red line in Fig. 4b). This polarization state persists even when the sensor returns to its ambient background condition because of the LRS along the reverse transfer curve. A coercive voltage -1.9 V for upward polarization state (erasing operation) is needed to reprogram information, which is far away from the assumed V_{ref} = -0.7 V. We also note here that the abovementioned non-volatile sensing can be achieved, without compromising any prospects of the CMOS compatibility and computing capability of the NC FeFET.

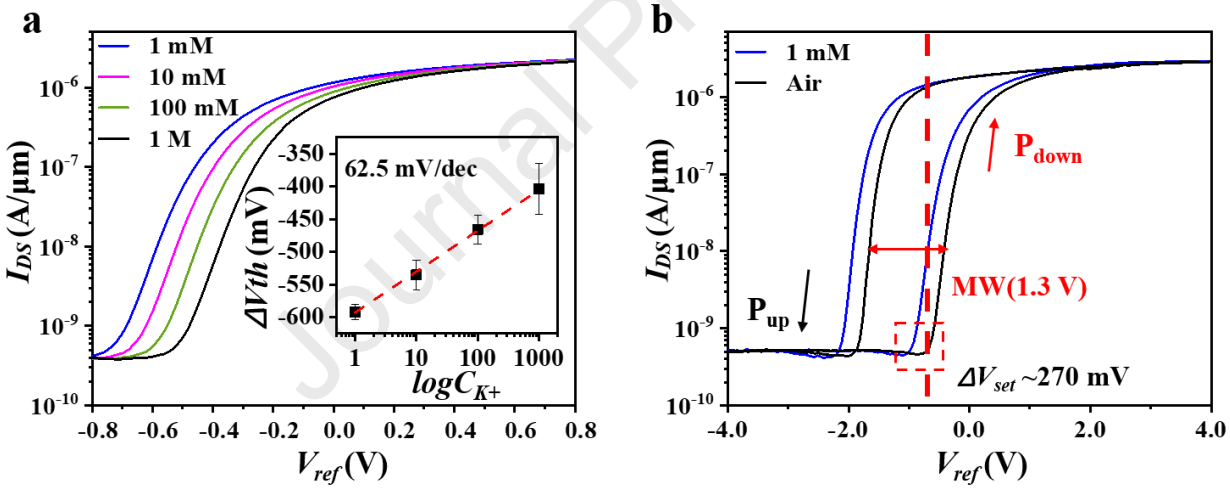

Fig. 4 | Sensitive, smart ion sensing response of HZO FeFETs. a, Transfer curves of n-type ferroelectric sensors in different concentrations KCl solutions from 1 mM to 1 M, shown by logarithmic scale. Inset: potassium response of the FeFET. **b,** Transfer characteristics (at 0.1 V V_{DS} and ±4 V gate range) under air and 1 mM solutions with relatively large memory windows of around 1.3 V. Inserted arrows indicate ferroelectric loop direction with the polarization state.

CONCLUSIONS

In summary, our study presents the demonstration of an HZO NC FeFET and its promising applications for sensing purposes in the form of EG ISFETs. The potassium ion-sensitive FeFETs exhibit a slightly supra-Nernst sensitivity of 62 (±2) mV/dec towards potassium ions, indicating their potential for highly sensitive ion detection. Furthermore, the incorporation of

a configurable non-volatile ferroelectric memory effect adds valuable memory retention and switching capabilities to the FeFETs, enhancing their versatility in sensing applications. This opens up exciting possibilities for the future development of diverse HZO NC FeFET biochemical sensor platforms in IoSMC applications.

REFERENCE

1. Chandrakasan, A. P., & Brodersen, R. W. Minimizing power consumption in digital CMOS circuits. PROCEEDINGS OF THE IEEE 83, 498-523 (1995). https://doi.org/10.1109/5.371964
2. Wang, S., Chen, X., Zhao, C., Kong, Y., Lin, B., Wu, Y., Bi, Z., Xuan, Z., Li, T., Li, Y., Zhang, W., Ma, E., Wang, Z., & Ma, W. An organic electrochemical transistor for multi-modal sensing, memory and processing. Nat. Electron. 6, 281-291 (2023). https://doi.org/10.1038/s41928-023-00950-y
3. Yu, J., Wang, Y., Qin, S., Gao, G., Xu, C., Lin Wang, Z., & Sun, Q. Bioinspired interactive neuromorphic devices. Mater. Today 60, 158-182 (2022). https://doi.org/https://doi.org/10.1016/j.mattod.2022.09.012
4. Lauks, I., Chan, P., & Babic, D. The extended gate chemically sensitive field effect transistor as multi-species microprobe. Sensors and Actuators 4, 291-298 (1983). https://doi.org/https://doi.org/10.1016/0250-6874(83)85035-5
5. Wei, W., Zeng, Z., Liao, W., Chim, W. K., & Zhu, C. Extended Gate Ion-Sensitive Field-Effect Transistors Using Al_2O_3/Hexagonal Boron Nitride Nanolayers for pH Sensing. ACS Applied Nano Materials 3, 403-408 (2020). https://doi.org/10.1021/acsanm.9b02037
6. Das, A., Ko, D. H., Chen, C.-H., Chang, L.-B., Lai, C.-S., Chu, F.-C., Chow, L., & Lin, R.-M. Highly sensitive palladium oxide thin film extended gate FETs as pH sensor. Sensors and Actuators B: Chemical 205, 199-205 (2014). https://doi.org/https://doi.org/10.1016/j.snb.2014.08.057
7. Pullano, S. A., Tasneem, N. T., Mahbub, I., Shamsir, S., Greco, M., Islam, S. K., & Fiorillo, A. S. Deep Submicron EGFET Based on Transistor Association Technique for Chemical Sensing. Sensors 19, 1063 (2019). https://doi.org/10.3390/s19051063
8. Catalan, G., Jimenez, D., & Gruverman, A. Negative capacitance detected. Nat. Mater. 14, 137-139 (2015). https://doi.org/10.1038/nmat4195
9. Salahuddin, S., & Dattat, S. Use of negative capacitance to provide voltage amplification for low power nanoscale devices. Nano Lett. 8, 405-410 (2008). https://doi.org/10.1021/nl071804g
10. Park, N., Kang, H., Park, J., Lee, Y., Yun, Y., Lee, J.-H., Lee, S.-G., Lee, Y. H., & Suh, D. Ferroelectric Single-Crystal Gated Graphene/Hexagonal-BN/Ferroelectric Field-Effect Transistor. ACS Nano 9, 10729-10736 (2015). https://doi.org/10.1021/acsnano.5b04339
11. Wang, X., Yu, P., Lei, Z., Zhu, C., Cao, X., Liu, F., You, L., Zeng, Q., Deng, Y., Zhu, C., Zhou, J., Fu, Q., Wang, J., Huang, Y., & Liu, Z. Van der Waals negative capacitance transistors. Nat. Commun. 10, 3037 (2019). https://doi.org/10.1038/s41467-019-10738-4
12. Si, M., Saha, A. K., Gao, S., Qiu, G., Qin, J., Duan, Y., Jian, J., Niu, C., Wang, H., Wu, W., Gupta, S. K., & Ye, P. D. A ferroelectric semiconductor field-effect transistor. Nat. Electron. 2, 580-586 (2019). https://doi.org/10.1038/s41928-019-0338-7
13. Miller, S. L., & McWhorter, P. J. Physics Of The Ferroeletric Nonvolatile Memory Field-effect Transistor. JOURNAL OF APPLIED PHYSICS 72, 5999-6010 (1992). https://doi.org/10.1063/1.351910
14. Mikolajick, T., Slesazeck, S., Park, M. H., & Schroeder, U. Ferroelectric hafnium oxide for ferroelectric

random-access memories and ferroelectric field-effect transistors. MRS Bulletin 43, 340-346 (2018). https://doi.org/10.1557/mrs.2018.92

15. Cheema, S. S., Shanker, N., Hsu, S.-L., Rho, Y., Hsu, C.-H., Stoica, V. A., Zhang, Z., Freeland, J. W., Shafer, P., Grigoropoulos, C. P., Ciston, J., & Salahuddin, S. Emergent ferroelectricity in subnanometer binary oxide films on silicon. Science 376, 648-+ (2022). https://doi.org/10.1126/science.abm8642
16. Trieloff, M., Jessberger, E. K., Herrwerth, I., Hopp, J., Fieni, C., Ghelis, M., Bourot-Denise, M., & Pellas, P. Structure and thermal history of the H-chondrite parent asteroid revealed by thermochronometry. Nature 422, 502-506 (2003). https://doi.org/10.1038/nature01499
17. Ambriz-Vargas, F., Kolhatkar, G., Broyer, M., Hadj-Youssef, A., Nouar, R., Sarkissian, A., Thomas, R., Gomez-Yáñez, C., Gauthier, M. A., & Ruediger, A. A Complementary Metal Oxide Semiconductor Process-Compatible Ferroelectric Tunnel Junction. ACS Appl. Mater. Interfaces 9, 13262-13268 (2017). https://doi.org/10.1021/acsami.6b16173
18. Khan, A. I., Keshavarzi, A., & Datta, S. The future of ferroelectric field-effect transistor technology. Nat. Electron. 3, 588-597 (2020). https://doi.org/10.1038/s41928-020-00492-7
19. Böscke, T. S., Müller, J., Bräuhaus, D., Schröder, U., & Böttger, U. Ferroelectricity in hafnium oxide thin films. Applied Physics Letters 99, 102903 (2011). https://doi.org/10.1063/1.3634052
20. Zarubin, S., Suvorova, E., Spiridonov, M., Negrov, D., Chernikova, A., Markeev, A., & Zenkevich, A. Fully ALD-grown TiN/$Hf_{0.5}Zr_{0.5}O_2$/TiN stacks: Ferroelectric and structural properties. Applied Physics Letters 109, 192903 (2016). https://doi.org/10.1063/1.4966219
21. Das, D., & Khan, A. I. Ferroelectricity in CMOS-Compatible Hafnium Oxides: Reviving the ferroelectric field-effect transistor technology. IEEE Nanotechnology Magazine 15, 20-32 (2021). https://doi.org/10.1109/MNANO.2021.3098218
22. Wang, J., Wang, D., Li, Q., Zhang, A., Gao, D., Guo, M., Feng, J., Fan, Z., Chen, D., Qin, M., Zeng, M., Gao, X., Zhou, G., Lu, X., & Liu, J. M. Excellent Ferroelectric Properties of $Hf_{0.5}Zr_{0.5}O_2$ Thin Films Induced by Al2O3 Dielectric Layer. IEEE Electron Device Lett. 40, 1937-1940 (2019). https://doi.org/10.1109/LED.2019.2950916
23. Guo, R., Zhou, Y., Wu, L., Wang, Z., Lim, Z., Yan, X., Lin, W., Wang, H., Yoong, H. Y., Chen, S., Ariando, Venkatesan, T., Wang, J., Chow, G. M., Gruverman, A., Miao, X., Zhu, Y., & Chen, J. Control of Synaptic Plasticity Learning of Ferroelectric Tunnel Memristor by Nanoscale Interface Engineering. ACS Appl. Mater. Interfaces 10, 12862-12869 (2018). https://doi.org/10.1021/acsami.8b01469
24. Xi, F., Han, Y., Liu, M., Bae, J. H., Tiedemann, A., Grützmacher, D., & Zhao, Q.-T. Artificial Synapses Based on Ferroelectric Schottky Barrier Field-Effect Transistors for Neuromorphic Applications. ACS Appl. Mater. Interfaces 13, 32005-32012 (2021). https://doi.org/10.1021/acsami.1c07505
25. Mueller, J., Boescke, T. S., Braeuhaus, D., Schroeder, U., Boettger, U., Sundqvist, J., Kuecher, P., Mikolajick, T., & Frey, L. Ferroelectric $Zr_{0.5}Hf_{0.5}O_2$ thin films for nonvolatile memory applications. APPLIED PHYSICS LETTERS 99, 112901 (2011). https://doi.org/10.1063/1.3636417
26. Tsai, S.-H., Fang, Z., Wang, X., Chand, U., Chen, C.-K., Hooda, S., Sivan, M., Pan, J., Zamburg, E., & Thean, A. V.-Y. Stress-Memorized HZO for High-Performance Ferroelectric Field-Effect Memtransistor. ACS Applied Electronic Materials 4, 1642-1650 (2022). https://doi.org/10.1021/acsaelm.1c01321
27. Bellando, F., Dabhi, C. K., Saeidi, A., Gastaldi, C., Chauhan, Y. S., & Ionescu, A. M. Subthermionic negative capacitance ion sensitive field-effect transistor. APPLIED PHYSICS LETTERS 116, 173503 (2020). https://doi.org/10.1063/5.0005411

28. Xu, J., Jiang, S.-Y., Zhang, M., Zhu, H., Chen, L., Sun, Q.-Q., & Zhang, D. W. Ferroelectric $HfZrO_x$-based MoS_2 negative capacitance transistor with ITO capping layers for steep-slope device application. APPLIED PHYSICS LETTERS 112, 103104 (2018). https://doi.org/10.1063/1.5019418
29. Tu, L., Cao, R., Wang, X., Chen, Y., Wu, S., Wang, F., Wang, Z., Shen, H., Lin, T., Zhou, P., Meng, X., Hu, W., Liu, Q., Wang, J., Liu, M., & Chu, J. Ultrasensitive negative capacitance phototransistors. Nat. Commun. 11, 101 (2020). https://doi.org/10.1038/s41467-019-13769-z
30. Chen, K. T., Chen, H. Y., Liao, C. Y., Siang, G. Y., Lo, C., Liao, M. H., Li, K. S., Chang, S. T., & Lee, M. H. Non-Volatile Ferroelectric FETs Using 5-nm $Hf_{0.5}Zr_{0.5}O_2$ With High Data Retention and Read Endurance for 1T Memory Applications. IEEE Electron Device Lett. 40, 399-402 (2019). https://doi.org/10.1109/LED.2019.2896231
31. Bhat, K. S., Ahmad, R., Mahmoudi, T., & Hahn, Y.-B. High performance chemical sensor with field-effect transistors array for selective detection of multiple ions. CHEMICAL ENGINEERING JOURNAL 417, 128064 (2021). https://doi.org/10.1016/j.cej.2020.128064
32. Zhang, J., Rupakula, M., Bellando, F., Cordero, E. G., Longo, J., Wildhaber, F., Herment, G., Guerin, H., & Ionescu, A. M. Sweat Biomarker Sensor Incorporating Picowatt, Three-Dimensional Extended Metal Gate Ion Sensitive Field Effect Transistors. ACS Sens. 4, 2039-2047 (2019). https://doi.org/10.1021/acssensors.9b00597
33. Aizawa, K., Park, B.-E., Kawashima, Y., Takahashi, K., & Ishiwara, H. Impact of HfO_2 buffer layers on data retention characteristics of ferroelectric-gate field-effect transistors. Applied Physics Letters 85, 3199-3201 (2004). https://doi.org/10.1063/1.1806274
34. Takahashi, K., Aizawa, K., Park, B.-E., & Ishiwara, H. Thirty-Day-Long Data Retention in Ferroelectric-Gate Field-Effect Transistors with HfO_2 Buffer Layers. Japanese Journal of Applied Physics 44, 6218-6220 (2005). https://doi.org/10.1143/jjap.44.6218
35. Ni, K., Sharma, P., Zhang, J., Jerry, M., Smith, J. A., Tapily, K., Clark, R., Mahapatra, S., & Datta, S. Critical Role of Interlayer in $Hf_{0.5}Zr_{0.5}O_2$ Ferroelectric FET Nonvolatile Memory Performance. IEEE Transactions on Electron Devices 65, 2461-2469 (2018). https://doi.org/10.1109/TED.2018.2829122
36. Zhou, J., Peng, Y., Han, G., Li, Q., Liu, Y., Zhang, J., Liao, M., Sun, Q. Q., Zhang, D. W., Zhou, Y., & Hao, Y. Hysteresis Reduction in Negative Capacitance Ge PFETs Enabled by Modulating Ferroelectric Properties in $HfZrO_x$. IEEE Journal of the Electron Devices Society, 6, 41-48 (2018). https://doi.org/10.1109/JEDS.2017.2764678
37. Wang, Y., Tao, L., Guzman, R., Luo, Q., Zhou, W., Yang, Y., Wei, Y., Liu, Y., Jiang, P., Chen, Y., Lv, S., Ding, Y., Wei, W., Gong, T., Wang, Y., Liu, Q., Du, S., & Liu, M.. A stable rhombohedral phase in ferroelectric $Hf(Zr)_{1+x}O_2$ capacitor with ultralow coercive field. Science, 381(6657), 558-563(2023). https://doi.org/10.1126/science.adf6137
38. Zhou, J., Wu, J., Han, G., Kanyang, R., Peng, Y., Li, J., Wang, H., Liu, Y., Zhang, J., Sun, Q. Q., Zhang, D. W., & Hao, Y. Frequency dependence of performance in Ge negative capacitance PFETs achieving sub-30 mV/decade swing and 110 mV hysteresis at MHz. 2017 IEEE International Electron Devices Meeting (IEDM), 15.5.1-15.5.4 (2017). https://doi.org/10.1109/IEDM.2017.8268397
39. Wang, C., Wu, J., Yu, H., Han, G., Miao, X., & Wang, X. Effects of Temperature on the Performance of $Hf_{0.5}Zr_{0.5}O_2$-Based Negative Capacitance FETs. IEEE Electron Device Letters, 41(11), 1625-1628 (2020). https://doi.org/10.1109/LED.2020.3022384
40. Krivokapic, Z., Rana, U., Galatage, R., Razavieh, A., Aziz, A., Liu, J., Shi, J., Kim, H. J., Sporer, R., Serrao,

C.,Busquet, A., Polakowski, P., Müller, J., Kleemeier, W., Jacob, A., Brown, D., Knorr, A., Carter, R., & Banna, S. 14nm Ferroelectric FinFET technology with steep subthreshold slope for ultra low power applications. 2017 IEEE International Electron Devices Meeting (IEDM), 15.11.11-15.11.14 (2017). https://doi.org/10.1109/IEDM.2017.8268393

41. Gao, J., Lian, X., Chen, Z., Shi, S., Li, E., Wang, Y., Jin, T., Chen, H., Liu, L., Chen, J., Zhu, Y., & Chen, W. Multifunctional $MoTe_2$ Fe-FET Enabled by Ferroelectric Polarization-Assisted Charge Trapping. Advanced Functional Materials 32, 2110415 (2022). https://doi.org/https://doi.org/10.1002/adfm.202110415
42. Íñiguez, J., Zubko, P., Luk'yanchuk, I., & Cano, A. Ferroelectric negative capacitance. Nature Reviews Materials 4, 243-256 (2019). https://doi.org/10.1038/s41578-019-0089-0
43. Li, Y., Liang, R., Wang, J., Jiang, C., Xiong, B., Liu, H., Wang, Z., Wang, X., Pang, Y., Tian, H., Yang, Y., & Ren, T. L. Negative Capacitance Oxide Thin-Film Transistor With Sub-60 mV/Decade Subthreshold Swing. IEEE Electron Device Lett. 40, 826-829 (2019). https://doi.org/10.1109/LED.2019.2907988
44. Kwon, D., Chatterjee, K., Tan, A. J., Yadav, A. K., Zhou, H., Sachid, A. B., Reis, R. D., Hu, C., & Salahuddin, S. Improved Subthreshold Swing and Short Channel Effect in FDSOI n-Channel Negative Capacitance Field Effect Transistors. IEEE Electron Device Lett. 39, 300-303 (2018). https://doi.org/10.1109/LED.2017.2787063
45. Wang, Y., Bai, X., Chu, J., Wang, H., Rao, G., Pan, X., Du, X., Hu, K., Wang, X., Gong, C., Yin, C., Yang, C., Yan, C., Wu, C., Shuai, Y., Wang, X., Liao, M., & Xiong, J. Record-Low Subthreshold-Swing Negative-Capacitance 2D Field-Effect Transistors. Adv. Mater. 32, 2005353 (2020). https://doi.org/10.1002/adma.202005353
46. Duarte, J. P., Khandelwal, S., Khan, A. I., Sachid, A., Lin, Y. K., Chang, H. L., Salahuddin, S., & Hu, C. Compact models of negative-capacitance FinFETs: Lumped and distributed charge models. 2016 IEEE International Electron Devices Meeting (IEDM)30.35.31-30.35.34 (2016). https://doi.org/10.1109/JEDS.2016.2632709.
47. Li, J., Zhou, J., Han, G., Liu, Y., Peng, Y., Zhang, J., Sun, Q. Q., Zhang, D. W., & Hao, Y. Correlation of Gate Capacitance with Drive Current and Transconductance in Negative Capacitance Ge PFETs. IEEE Electron Device Lett. 38, 1500-1503 (2017). https://doi.org/10.1109/LED.2017.2746088

MISCELLANEA

Data Availability Statement: The data that supports the findings of this study are available within the article [and its supplementary material].

Acknowledgments: Financial support from the National Natural Science Foundation of China No. 52073160 and the National Key Research and Development Program of China No. 2020YFF01014706 is gratefully acknowledged.

Conflicts of Interest: The authors declare no conflict of interest.

Conflicts of Interest: The authors declare no conflict of interest.